A&A manuscript no.
(will be inserted by hand later)

Your thesaurus codes are:
02.02.1 – 02.18.5 – 11.01.2 – 11.14.1 – 13.07.1

ASTRONOMY
AND
ASTROPHYSICS
1.2.2008

Reverberation mapping of the central regions of active galactic nuclei using high-energy γ-ray observations

M. Böttcher[1] **and C. D. Dermer**[2]

[1] Max-Planck-Institut für Radioastronomie, Postfach 2024, 53010 Bonn, Germany
[2] E. O. Hulburt Center for Space Research, Code 7653, Naval Research Laboratory, Washington, DC 20375-5352, USA

Recieved ; accepted

Abstract. We calculate the time- and energy-dependent opacity of high-energy γ-rays attenuated by pair-production interactions with accretion-flare photons that are scattered by gas and dust surrounding the nuclei of active galaxies. We show that the temporal behavior of the high-energy opacity cutoff can be used in conjunction with the time history of the accretion flare to determine the location of the γ-ray emission site, as well as the column density and scale height of the material surrounding the central engine. Reverberation mapping using this technique is now possible for nearby BL Lac objects such as Mrk 421, and will be particularly valuable when the 10 GeV – 100 GeV γ-ray window is opened, because here the attenuation of distant blazar radiation by the intergalactic infrared background radiation is negligible.

Key words: Galaxies: nuclei – galaxies: active – gamma rays: galaxies – black hole physics

1. Introduction

Markarian 421, a BL Lac object with redshift $z = 0.031$, is the first extragalactic object detected at TeV energies with high significance (Punch et al. 1992). Searches for other AGNs emitting VHE γ-rays have been conducted using the air Cerenkov telescopes of the *Whipple Observatory* (Schubnell et al. 1994). These searches have naturally focused on those extragalactic γ-ray sources already detected at photon energies $E > 100$ MeV with the EGRET instrument on the *Compton Gamma Ray Observatory* (Fichtel et al. 1994; Dermer & Gehrels 1995), but have so far yielded negative results. Two explanations have been advanced to explain these observations. Because Mrk 421 is so close by cosmological standards, its detection, coupled with the failure to detect more distant blazars, implies that TeV γ-rays from the more distant objects are attenuated by the diffuse intergalactic infrared radiation field (Stecker, de Jager, & Salamon 1992; de Jager, Stecker, & Salamon 1994). By contrast, Dermer & Schlickeiser (1994) point out that BL Lac is a truly lineless object (see, e.g., Kikuchi & Mikami 1987), and as such has only very tenuous emission line clouds near the central engine compared to the stong emission lines found in quasars (and some BL Lac objects). Thus the rescattered central source radiation is very dilute in Mrk 421, permitting the TeV γ-rays to escape without attenuation.

In 1994 May, Mrk 421 was observed to flare in TeV γ-rays during a period of $\sim$ 2 days by a factor of 10 over its flux level in the period 1994 Jan.-Apr., or by a factor of 5 above its quiescent flux level measured in 1992 and 1993 (Kerrick et al. 1995; Macomb et al. 1995). Observations with *ASCA* made 2 days after the onset of the TeV γ-ray flare also showed an enhanced level of 2-10 keV X-rays compared with earlier *EXOSAT* measurements (Takahashi et al. 1994). These observations suggest a method to diagnose the structure and density of the gas and dust surrounding the central source of Mrk 421 and other γ-ray blazars. By monitoring the time dependence of the flaring emission from the central source and the pair attenuation cutoff of the high energy γ-rays due to photon-photon pair production, we can extract information about the column density, number density, and location of the site of high-energy γ-ray production. This is a new example of a reverberation mapping technique which uses correlated temporal signatures to monitor conditions of a physical system, analogous to methods where variability of emission line intensities are monitored in response to the temporal behavior of photoionizing radiation from the central source (cf. Peterson et al. 1991).

In Section 2, we describe the system and model it under the assumption that the central source radiation can be approximated by a point source. Asymptotic forms for the total photon number density and opacity at times long after the peak of the flare are derived in Section 3, and

Send offprint requests to: M. Böttcher

numerical simulations are presented in Section 4. We summarize in Section 5.

2. Time-dependence of photon opacity from scattered radiation

Attenuation of MeV-TeV γ-rays by photons with energies in the infrared through X-ray range can occur in the central regions of active galactic nuclei if both the intensity of the lower energy radiation and the scattering depth of the surrounding medium are sufficiently great, provided that the spatial extent of the scattering medium is not too large (e.g., Blandford 1993; Dermer & Schlickeiser 1994; Blandford & Levinson 1995). The presence of strong emission lines from quasars implies the existence of surrounding clouds of gas which can rescatter the central-source radiation (Sikora, Begelman, & Rees 1994). The structure and column density of the surrounding gas near the supermassive black holes powering quasars is, however, not well known. Information about the location of the γ-ray emission site and the spatial extent and density of gas and dust surrounding the supermassive black hole can be extracted using the method we now describe.

We consider the attenuation of γ-rays emitted outward along the z-axis at height z_i above a central soft-photon source (e. g., an accretion disk) which exhibits a flare described, for simplicity, by a Gaussian in time:

$$\dot{N}_{ph}(\epsilon,\Omega;t) = \dot{N}_{max}(\epsilon,\Omega)\, e^{-\frac{t^2}{2\sigma^2}} \ . \qquad (1)$$

In eq. (1), $\dot{N}_{ph}(\epsilon,\Omega;t)d\epsilon d\Omega$ is the differential number of photons emitted per second at time t with dimensionless energy $\epsilon \equiv h\nu/\mathrm{m}_e\mathrm{c}^2$ in the range ϵ and $\epsilon + d\epsilon$ that are directed into the solid angle element $d\Omega$ in the direction $\Omega = (\theta,\phi)$. The full-width half maximum duration of the flare is given by $2^{3/2}(\ln 2)\sigma \cong 1.96\sigma$, and the photon emissivity at the peak of the flare is denoted by $\dot{N}_{max}(\epsilon,\Omega)$. Some of these soft photons are scattered by surrounding clouds of density $n_e(\mathbf{r})$ into the path of the γ-rays. The scattered soft photons are directed at an angle $\theta^* = \cos^{-1}\mu^*$ with respect to the z-axis, as shown in Figure 1. We assume that the gas is moving nonrelativistically and can be treated as a stationary scattering medium. We also assume that the gas is optically thin to Thomson scattering so that only single scatterings are important.

The opacity of a photon with dimensionless energy ϵ_1 due to photon-photon pair production can be written as

$$\tau_{\gamma\gamma}(\epsilon_1,t_i,z_i) = \int_{z_i}^{\infty} dz \int_0^{2\pi} d\phi^* \int_{-1}^{1} d\mu^*(1-\mu^*) \int_{\frac{2}{\epsilon_1(1-\mu^*)}}^{\infty} d\epsilon\cdot$$

$$\cdot\sigma_{\gamma\gamma}(\epsilon_1,\epsilon,\mu^*)\, n_{ph}(\epsilon,\mu^*,\phi^*;z,t_i+\frac{z-z_i}{c}). \qquad (2)$$

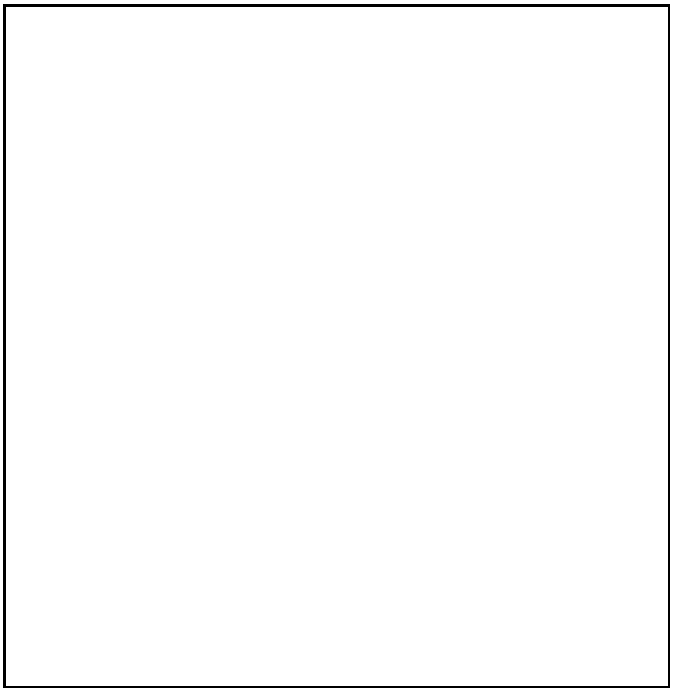

Fig. 1. Geometry of the system. Soft photons are emitted at time t from an accretion disk which is approximated by a point source at the origin. The photons are Thomson-scattered at location $\mathbf{r}$ by electrons in surrounding dust and gas clouds. The scattered radiation intercepts high-energy photons which are beamed outward along the z-axis, and contribute to the opacity of the high-energy gamma rays through $\gamma-\gamma$ pair production attenuation.

(Gould & Schréder 1967; for corrections see Brown, Mikaelian, & Gould 1973). Here t_i denotes the emission time of the high-energy photon, $n_{ph}(\epsilon,\mu^*,\phi^*;z,t)$ represents the spectral density of scattered soft photons per unit solid angle at height z and time t, and the pair production cross section is given by

$$\sigma_{\gamma\gamma}(\beta) = \frac{3}{16}\sigma_T(1-\beta^2)\cdot$$

$$\cdot[(3-\beta^4)\ln\left(\frac{1+\beta}{1-\beta}\right) - 2\beta(2-\beta^2)] \qquad (3)$$

where

$$\beta = \sqrt{1-\frac{2}{\epsilon\epsilon_1(1-\mu^*)}} \qquad (4)$$

is the velocity of the electron/positron in the center-of-momentum frame.

The soft photon density per unit solid angle at location $\mathbf{r}$ in the direction $\overline{\Omega} = (\theta,\phi)$ defined by the location of the scattering material relative to the position of the soft photon source is given by

$$n_{ph}(\epsilon,\Omega;\mathbf{r},t) = \frac{\dot{N}_{ph}(\epsilon,\Omega;t-\frac{r}{c})}{r^2\,c}\,\delta(\Omega-\overline{\Omega}). \qquad (5)$$

We approximate the Thomson scattering event by isotropic scattering with cross section σ_T and neglect recoil, which is a good approximation when $\epsilon \ll 1$. The photon production rate by Thomson scattering at location $\mathbf{r}$ and time t is therefore

$$\dot{n}_{ph}(\epsilon_s,\Omega_s;\mathbf{r},t) = \frac{\sigma_T}{4\pi r^2}\,n_e(\mathbf{r})\dot{N}_{ph}\left(\epsilon_s,\overline{\Omega};t-\frac{r}{c}\right), \qquad (6)$$

where the subscript "s" is used to denote the scattered quantities.

Because the particles at each point in the cloud are assumed to scatter isotropically, the spectral density of scattered photons at height z along the z-axis and at time t can be obtained by integrating the scattered spectrum over all space. We find that

$$n_{ph}(\epsilon;z,t) = \frac{\sigma_T}{4\pi c}\int_0^{2\pi} d\phi \int_{-1}^{1} d\mu \int_0^{\infty} dr\;\frac{n_e(\mathbf{r})}{x^2}\cdot$$

$$\cdot\dot{N}_{ph}\left(\epsilon,\Omega;t-\frac{r+x}{c}\right), \qquad (7)$$

where we have dropped the subscript denoting scattered quantities, and the overbar on Ω in the expression for $\dot{N}_{ph}$. It is then a simple matter to obtain the angle-dependence of the photon spectral density through the expression

$$n_{ph}(\epsilon,\mu^*,\phi^*;z,t) = \frac{\sigma_T}{4\pi c}\int_{-1}^{1} d\mu \int_0^{\infty} dr\;\frac{n_e(\mathbf{r})}{x^2}\cdot$$

$$\cdot\dot{N}_{ph}\left(\epsilon,\Omega;t-\frac{r+x}{c}\right)\delta(\phi^*-\bar{\phi}^*)\delta\big(\mu^*-\overline{\mu}^*[r,\mu,x]\big). \qquad (8)$$

Here $x = (r^2+z^2-2rz\mu)^{1/2}$ is the distance between the scattering electron and the z-axis at height z, the angle $\overline{\mu}^*$ is given by

$$\overline{\mu}^* = \sqrt{1-\left(\frac{r}{x}\right)^2(1-\mu^2)}\;, \qquad (9)$$

and the angle $\bar{\phi}^* = \pi+\phi$ (see Fig. 1). Substituting equation (8) into equation (2), assuming azimuthal symmetry of the soft-photon emission spectrum and distribution of scattering material, gives the photon opacity

$$\tau_{\gamma\gamma}(\epsilon_1,t_i,z_i) = \frac{\sigma_T}{2c}\int_{z_i}^{\infty} dz \int_{-1}^{1} d\mu^*(1-\mu^*) \int_{\frac{2}{\epsilon_1(1-\mu^*)}}^{\infty} d\epsilon\;\sigma_{\gamma\gamma}(\beta)\cdot$$

$$\cdot\int_{-1}^{1} d\mu \int_0^{\infty} dr\;\frac{n_e(\mathbf{r})}{x^2}\dot{N}_{ph}\left(\epsilon,\Omega;t_i+\frac{z-z_i-r-x}{c}\right)\delta\big(\mu^*-\overline{\mu}^*\big). \qquad (10)$$

In order to perform the μ^*-integration by evaluating the δ-function it is necessary to change the order of integrations. The limits for the remaining integrals then follow from the threshold condition

$$\epsilon\epsilon_1(1-\overline{\mu}^*) > 2, \qquad (11)$$

and we find

$$\tau_{\gamma\gamma}(\epsilon_1,t_i,z_i) = \frac{\sigma_T}{2c}\int_{z_i}^{\infty} dz \int_{\frac{1}{\epsilon_1}}^{\infty} d\epsilon \int_{-k}^{1} d\mu \int_{r_{min}}^{\infty} dr\;\frac{n_e(\mathbf{r})}{x^2}(1-\bar{\mu}^*)\cdot$$

$$\cdot\sigma_{\gamma\gamma}(\epsilon,\epsilon_1,\overline{\mu}^*)\;\dot{N}_{ph}\left(\epsilon,\Omega;t_i+\frac{z-z_i-r-x}{c}\right), \qquad (12)$$

where

$$r_{min} = z\sqrt{1-k^2}\;\left(\frac{\mu\sqrt{1-k^2}-k\sqrt{1-\mu^2}}{\mu^2-k^2}\right) \qquad (13)$$

if $\mu^2 \neq k^2$, and

$$k \;=\; 1-\frac{2}{\epsilon\,\epsilon_1}. \qquad (14)$$

If $\mu = k$ we have $r_{min} = \frac{z}{2k}$ (for this case $k > 0$ is required), while for $\mu = -k$ condition (11) can not be satisfied ($r_{min} \to \infty$).

To illustrate the importance of the effect of photon attenuation by reverberating soft photons, we assume that the disk radiates isotropically and that its radiation during the flare is described by a power law in photon energy described by the expression

$$\dot{N}_{ph}(\epsilon,\Omega;t) = \frac{K\,\epsilon^{-\alpha}}{4\pi}\,e^{-\frac{t^2}{2\sigma^2}}\;, \qquad (15)$$

with cutoff energies ϵ^l and ϵ^u. The power-law spectra could be produced in the inner hot regions of an accretion disk by nonthermal electrons which radiate synchrotron photons at frequencies above the self-absorption frequency. A more detailed model of the flaring emission from an accretion disk would require time-dependent solutions of the accretion disk equations (see, e.g., White & Lightman 1990), which we neglect for simplicity. We also assume for purposes of illustration that the surrounding clouds are homogeneously distributed with uniform density $n_e(\mathbf{r}) = n_o$.

The constant K is related to the maximum luminosity of the disk by

$$K = \begin{cases} \frac{2-\alpha}{m_e\,c^2}\,\frac{10^{46}L_{46}\mathrm{ergs\ s^{-1}}}{(\epsilon^u)^{2-\alpha}-(\epsilon^l)^{2-\alpha}} & \text{for } \alpha \neq 2 \\ \frac{10^{46}L_{46}\mathrm{ergs\ s^{-1}}}{m_e\,c^2}\ln(\epsilon^u/\epsilon^l) & \text{for } \alpha = 2 \end{cases}, \qquad (16)$$

where L_{46} is the maximum disk luminosity in units of 10^{46} ergs s^{-1} and $m_e c^2$ is the electron rest mass energy in ergs.

3. Asymptotic behavior of photon density and opacity

If we consider the effects of reverberation at times much later than the flare maximum, considerable simplifications of the exact expressions (7) and (12) for the scattered photon density and opacity, respectively, are possible. The derived asymptotic expressions provide useful checks on the numerical results presented in the next section.

Under the assumptions made at the end of the previous section, we may write the total scattered photon density as

$$n_{ph}(\epsilon;z,t) = \frac{n_0\,\sigma_T\,K\,\epsilon^{-\alpha}}{8\,\pi\,c\,z}\int\limits_0^\infty dr \int\limits_{|r-z|}^{r+z} dx\,\frac{e^{-\frac{\left(t-\frac{x+r}{c}\right)^2}{2\sigma^2}}}{x\,r}\ . \quad (17)$$

At times $t \gg \sigma$ and $t \gg \frac{z}{c}$, equation (16) reduces to

$$n_{ph}(\epsilon;z,t) \approx \frac{n_0\,\sigma_T\,K\,\epsilon^{-\alpha}}{8\,\pi\,c\,z}\int\limits_0^\infty dr \int\limits_{-\infty}^{\infty} dx\,\frac{e^{-\frac{(x-x_0)^2}{2\,\sigma^2\,c^2}}}{x_0\,r}\cdot$$

$$\cdot\Theta(r+z-x_0)\,\Theta(x_0-|r-z|)\ , \quad (18)$$

where $x_0 = ct - r$ and Θ denotes the Heaviside function such that $\Theta(y) = 1$ if $y \geq 0$ and $\Theta(y) = 0$ otherwise. Thus, we have

$$n_{ph}(\epsilon;z,t) \approx \frac{n_0\,\sigma_T\,K\,\epsilon^{-\alpha}}{8\,\pi\,c\,z}\,\sqrt{2\,\pi\,\sigma^2\,c^2}\int\limits_{\frac{ct-z}{2}}^{\frac{ct+z}{2}}\frac{dr}{r}\,\frac{1}{ct-r}$$

$$= \frac{n_0\,\sigma_T\,K\,\epsilon^{-\alpha}}{4\,\pi\,c\,z}\,\frac{\sqrt{2\,\pi\,\sigma^2\,c^2}}{ct}\,\ln\left(\frac{ct+z}{ct-z}\right)$$

$$\approx \frac{n_0\,\sigma_T\,K\,\epsilon^{-\alpha}}{2\,\pi}\,\frac{\sqrt{2\,\pi\,\sigma^2}}{(ct)^2}\ . \quad (19)$$

Note that this last expression does not explicitly depend on z.

Inserting this expression into eq. (2), we set $t = t_i + \frac{z-z_i}{c}$, noting that approximation (19) is valid for $ct \gg z_i$. The disk photon density at the location of the scattering electrons decreases as $\frac{1}{r^2}$ and the scattered photon density, again, decreases as $\frac{1}{x_0^2}$. Therefore, the main contribution of scattered photons will come from that angle θ^* with respect to the z-axis for which $x_0 = r$. This yields

$$\mu_0^* = \frac{z}{ct_i + z - z_i}. \quad (20)$$

Using the scattered photon density

$$n_{ph}(\epsilon,\mu^*,\phi^*;z,t) \approx (2\pi)^{-1} n_{ph}(\epsilon;z,t)\delta(\mu^*-\mu_0^*)\ , \quad (21)$$

we find

$$\tau_{\gamma\gamma}(\epsilon_1,t_i) \cong \frac{n_0 K \sigma_T \sigma}{\sqrt{2\pi}}\ (ct_i - z_i)\cdot$$

$$\cdot\int\limits_{z_i}^{\infty}\frac{dz}{(ct_i+z-z_i)^3}\int\limits_{\frac{2}{\epsilon_1(1-\mu_0^*)}}^{\epsilon^u} d\epsilon\,\epsilon^{-\alpha}\,\sigma_{\gamma\gamma}(\epsilon_1,\epsilon,\mu_0^*)$$

$$= \frac{2n_0 K\sigma_T\sigma}{\sqrt{2\pi}}\,\left(\frac{\epsilon_1}{2}\right)^{\alpha-1}\int\limits_{z_i}^{\infty}\frac{dz}{(ct_i+z-z_i)^2}\cdot$$

$$\cdot(1-\mu_0^*)^\alpha\int\limits_{\beta_{min}}^{\beta_{max}} d\beta\,\beta\,(1-\beta^2)^{\alpha-2}\,\sigma_{\gamma\gamma}(\beta) \quad (22)$$

where

$$\beta_{min} = \begin{cases}\sqrt{1-\frac{2}{\epsilon_1\epsilon^l(1-\mu_0^*)}} & \text{if } \epsilon^l > \frac{2}{\epsilon_1(1-\mu_0^*)} \\ 0 & \text{otherwise}\end{cases}\ , \quad (23a)$$

and

$$\beta_{max} = \sqrt{1-\frac{2}{\epsilon_1\epsilon^u(1-\mu_0^*)}}\ . \quad (23b)$$

Here we may assume $\beta_{min} \approx 0$, $\beta_{max} \approx 1$ for the model we consider, because the pair production cross section (3) vanishes for $\beta \to 0$ and for $\beta \to 1$.

The z-integration in eq. (22) can easily be done analytically, and the second integration is only dependent on the spectral index α. Thus, we define

$$I(\alpha) \equiv \int\limits_0^1 d\beta\,\beta\,(1-\beta^2)^{\alpha-2}\,\sigma_{\gamma\gamma}(\beta) \quad (24)$$

$$I(1.5) \approx 0.3\,\sigma_T$$

The function $I(\alpha)$ is only weakly dependent on α. The photon opacity for times late after the flare is given by

$$\tau_{\gamma\gamma}(\epsilon_1,t_i) = \frac{2^{1/2}\,n_0\,K\,\sigma_T\,\sigma}{\pi^{1/2}}\,\frac{1}{\alpha+1}\,\left(\frac{\epsilon_1}{2}\right)^{\alpha-1}\frac{1}{ct_i}\,I(\alpha)\ , \quad (25)$$

which is independent of z_i because we neglected z_i compared to ct_i in equation (25).

4. Numerical Results

We now show the results of numerically performing the integrals (7) and (12), and compare these results with approximations (19) and (25), respectively, derived in Section 3. We assume that the medium surrounding the central engine has a Thomson scattering optical depth of 0.02, extends out to a scale height of 0.1 pc, and is uniformly distributed in this region. This yields an electron density $n_0 = 10^5$ cm^{-3}. Furthermore, we describe the disk photon spectrum during the flare by a power law with spectral index $\alpha = 1.5$ extending from dimensionless photon energy $\epsilon^l = 10^{-8}$ (corresponding to $5 \cdot 10^{-3}$ eV) to $\epsilon^u = 10^{-2}$ ($5 \cdot 10^3$ eV), and assume its maximum luminosity $L_{max} = 10^{46}$ ergs s^{-1}.

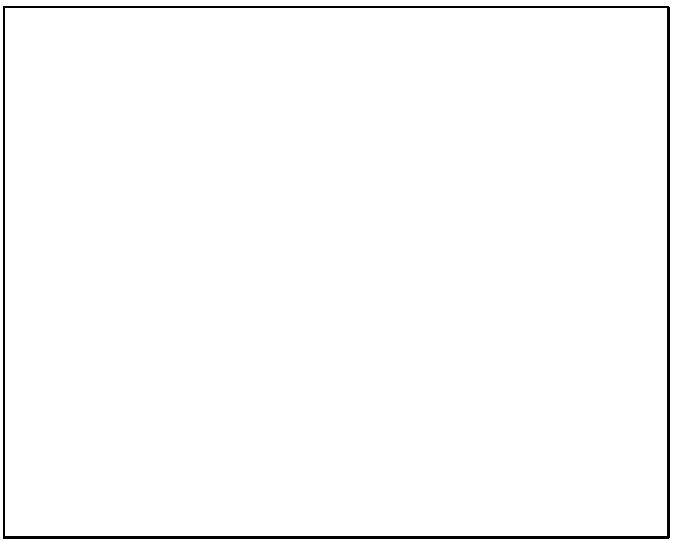

Fig. 2. Time dependence of the scattered photon number density and pair-production opacity $\tau_{\gamma\gamma}$. The photon number density is computed at $z = 10^{-2}$ pc, and $\tau_{\gamma\gamma}$ is for a 500 GeV photon ($\epsilon_1 = 10^6$) interacting with lower-energy photons produced in an accretion-disk flare described by a Gaussian in time with a full-width half-maximum duration of one week. The approximations valid at late time are shown by the dotted curves.

The time-dependent effect of a one-week flare described by equation (15) on the pair-production opacity for 500 GeV photons ($\epsilon_1 = 10^6$) emitted at $z_i = 10^{-2}$ pc, together with the total scattered-photon number density at the injection height, is shown in Fig. 2. We see that the photon opacity reaches maximum values of order unity and, due to the finite light travel time, attains its maximum at times later than at $t = z_i/c$ which, for the example considered here, is $\sim 10^6$ s. The numerical results show good agreement with the approximations for the asymptotic behavior at late times, which indicates a decrease of the opacity as $1/t$. If $ct > 0.1$ pc ($t \gtrsim 10^7$ s), of course, the numerical results will decrease faster than the approximation because the latter does not take into account the lack of scattering material at $r > 0.1$ pc.

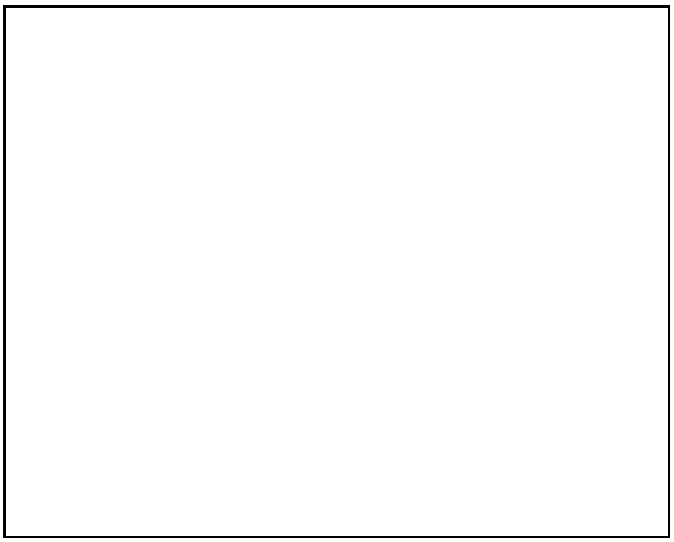

Fig. 3. Time dependence of the pair-production opacity $\tau_{\gamma\gamma}$ for photons emitted at different heights z_i given by the labels on the curves. Other parameters are the same as in Fig. 2. The dotted curve shows approximation (25) for $\tau_{\gamma\gamma}$.

In Fig. 3 we show the dependence of the photon opacity on the injection height z_i, with all other parameters the same as given in the case shown in Fig. 2. From variability time scale arguments, Kerrick et al. (1995) derived an upper limit of 0.03 pc on the size of the emitting region of the TeV radiation for the case of Mrk 421. This is in accord with the values of z_i used in Fig. 3 if the injection height and inferred size scale are comparable. As the injection height increases, the maximum photon opacity decreases and attains its greatest value at increasingly later times. It is interesting to note that, as we already saw from equation (25), the photon opacity late after the flare maximum does not depend on the injection height. Note also that the delay between $t = z_i/c$ and the time of maximum opacity depends very weakly on the injection height. In the case considered here, the delay $\Delta t \approx 10^6$ s, corresponding to the duration of the flare.

The energy dependence of the opacity $\tau_{\gamma\gamma}$ is shown in Fig. 4 where, again, the dotted curves represent the analytic approximation (25). For these calculations, we assumed an injection height of $z_i = 10^{-3}$ pc. From this figure, we see that the form of the time-dependent photon opacity is esentially the same at all gamma-ray energies. The relative amplitude of the opacity curves is described by

$$\tau_{\gamma\gamma}(\epsilon_1, t_i) \propto \epsilon_1^{\alpha-1} \,, \tag{26}$$

as was shown for the asymptotic behavior (eq. [25]).

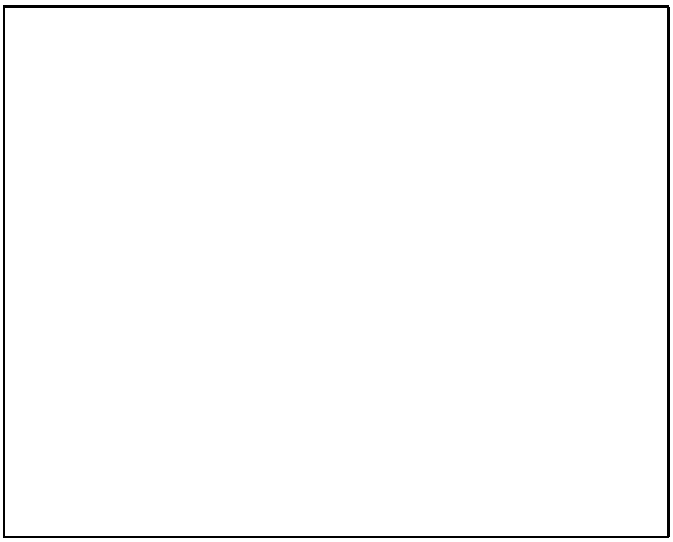

Fig. 4. Time dependence of the pair-production opacity $\tau_{\gamma\gamma}$ for photons emitted at height $z_i = 10^{-3}$ pc with dimensionless energies ϵ_i given by the labels on the curves. Other parameters are the same as in Fig. 2. The dotted curves show approximation (25) for $\tau_{\gamma\gamma}$.

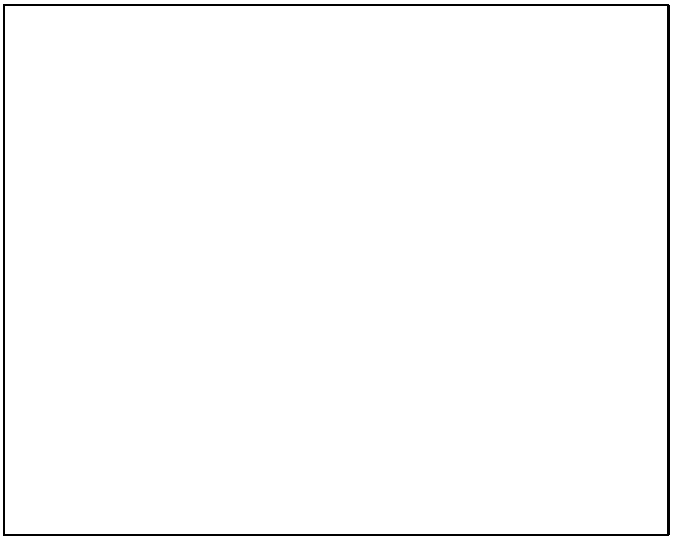

Fig. 5. Time dependence of the observed photon spectrum due to photon-photon attenuation by soft photons from an accretion-disk flare which are scattered into the high-energy photon beam. Here we assume a power-law photon spectrum with photon spectral index $\alpha = 2$. The high-energy photons are assumed to be emitted at height $z_i = 10^{-3}$ pc. Other parameters are the same as in Fig. 2. The curves are labeled by time after flare maximum.

Fig. 5 shows the time-dependent modification of a primary γ-ray spectrum by the effects of pair-production opacity effects from accretion disk-flare photons. Here we let the primary gamma-ray spectrum be described by a power law with spectral index $\alpha = 2.0$, and choose an emission height $z_i = 10^{-3}$ pc. The results are plotted for different times with respect to the time of the maximum of the accretion-disk flare. As can be seen, γ-rays with energies $\gtrsim 500$ GeV will be almost completely absorbed after $\sim 10^4$ s following the flare maximum and will remain strongly attenuated long after the flare. If we assume a greater injection height, this effect will occur correspondingly later and the influence of reverberating photons will be restricted to higher energy γ-rays, as can be seen from Fig. 4.

5. Discussion and Summary

We have considered a highly simplified geometry to illustrate the potential of gamma-ray astronomy to map the structure and density of clouds of dust and gas surrounding the central nucleus of a BL Lac object or quasar. Photon-photon attenuation intrinsic to the source will occur only if the surrounding medium has a sufficiently large column density or if the gamma-ray emission site is sufficiently near the central nucleus. As pointed out in the Introduction, the scattering emission line clouds are relatively tenuous in Mrk 421 compared to quasars. It is therefore likely that the number density of the scattering medium in Mrk 421 is significantly less than 10^5 cm^{-3}, the value assumed in our model calculations. As the pair production optical depth scales roughly linearly with the number density of the scattering material, this is consistent with the observational result by Kerrick et al. (1995), who did not find any temporal variation of the spectral shape during the TeV γ-ray flare in 1994 May.

This observation implies a limit on the density of the scattering material surrounding the central engine of Mrk 421 if the TeV γ-ray production site is within 0.03 pc (see Section 4). Using Eq. (26) and the results shown in Fig. 3, and assuming that the pair production optical depth up to several TeV ($\epsilon_1 \sim 10^7$) always remained less than 0.1, we find that

$$n_0 \lesssim 10^4\, \epsilon_1^{1-\alpha}\, L_{46}^{-1}\ \mathrm{cm}^{-3} \approx 3\, L_{46}^{-1}\ \mathrm{cm}^{-3} \qquad (27)$$

for a Gaussian flare with a FWHM duration of 1 week. Optical and TeV gamma-ray campaigns to monitor Mrk 421 can therefore provide constraints on the density of the surrounding medium of Mrk 421. During the May 1994 outburst of Mrk 421, however, only variations in the keV and TeV ranges were observed, whereas no significant variations were seen in near-simultaneous mm, IR, UV, and GeV gamma-ray observations (Macomb et al. 1995). The keV X-rays are most effective in attenuating 0.1- 1 GeV gamma rays. We could apply our results to this regime, noting that the X-ray flare luminosity was at the level of

$\sim 2 \cdot 10^{44}$ ergs s^{-1}. Although the poor statistics of GeV observations might not support a constraint as strong as $\tau_{\gamma\gamma} \lesssim 0.1$, equation (27) should yield a sensible estimate for this case. This implies a density of $n_0 \lesssim 10^4$ cm^{-3} for a one week X-ray flare, corresponding to a Thomson scattering optical depth of $\tau_T \lesssim 0.002$ of the surrounding scattering medium if it exends out to a scale height of 0.1 pc. Accounting for probable inhomogeneities (e. g., a decrease of the cloud density with distance from the center) together with the relatively high location of the γ-ray emission site, this limit on the Thomson scattering optical depth should be raised somewhat in order to yield a more conservative estimate. It should be kept in mind, however, that the X-ray flare in this event is probably beamed emission from the jet, in which case these estimates do not apply.

As shown in Fig. 5, the time-dependent truncation of the gamma-ray spectra following an accretion-disk flare gives useful information about the location of the gamma-ray emission region and the mean density of the surrounding gas and dust. By comparing the temporal behavior of the flare and the attenuated gamma-ray spectrum in detail, further information about the distribution of scattering gas can be obtained.

We can predict idealized time-dependent behavior of γ-ray emission in response to variations in the lower-energy radiation for specific models. In the models of Dermer & Schlickeiser (1993) and Sikora et al. (1994), gamma-ray production in blazars is caused by Compton scattering of accretion-disk photons or rescattered radiation. Flaring accretion-disk radiation in the infrared to X-ray range will produce flaring behavior at 100 MeV to GeV energies due to the time-variable soft photon energy density in the relativistically outflowing fluid frame. If there are extremely energetic electrons in the fluid frame, then a flare can also occur in the TeV range. The shape of the unabsorbed IC-spectrum has been calculated for isotropic relativistic electrons in the outflowing fluid frame (Dermer & Schlickeiser 1993). If the accretion-disk flaring behavior in the infrared and optical range shows the same behavior as the UV/X-ray flare, then the γ-ray spectrum will be absorbed according to the time and energy dependence illustrated in Fig. 5.

It is important to note that it is the infrared and optical photons that are most effective in attenuating TeV gamma rays (e.g., Stecker et al. 1992). To apply our method to TeV measurements, therefore, correlated infrared/optical and high-energy gamma-ray observations are necessary (note that no space-based detectors may be necessary in this case). However, the diffuse intergalactic infrared background radiation produced by the superposition of reprocessed emission from stellar nucleosynthesis renders most quasars with redshifts $\gtrsim 0.2$ invisible, due to strong $\gamma - \gamma$ attenuation over this pathlength (see also Stecker & de Jager 1993; MacMinn & Primack 1994). For applications to a larger number of objects, it is therefore desirable to devise γ-ray detection systems in the 10 GeV - several hundred GeV regime, where the effects of the diffuse infrared background radiation are small. The identification of attenuation intrinsic to the source will be necessary, in any case, to implement methods to infer the Hubble constant from high-energy gamma-ray observations (Salamon, Stecker, & De Jager (1994)).

Finally, we note that the presence of scattered radiation in the source will confuse any attempt to determine the level of the intergalactic infrared background radiation using high energy γ-ray observations of blazars (Stecker et al. 1992; Dermer & Schlickeiser 1994). By monitoring temporal variations at low and high-photon energies, our method provides a way to subtract out the level of attenuation intrinsic to the source, and determine whether the diffuse intergalactic infrared background or rescattered radiation is more important for attenuating high-energy photons in a given source.

Acknowledgements. We thank Dr. R. Schlickeiser for comments and discussions. Useful comments by Dr. John Mattox and the referee, Professor O. C. de Jager, are also acknowledged. Partial support for the work of C. D. was provided under NASA grant DPR S-30931-F. M. Böttcher acknoledges financial support by the Deutsche Forschungsgemeinschaft.

References

Blandford, R. D. 1993, in Compton Gamma-Ray Observatory, ed. M. Friedlander, N. Gehrels, and D. J. Macomb (New York: AIP), p. 533
Blandford, R. D., and Levinson, A. 1995, ApJ, in press
Brown, R. W., Mikaelian, K. O., & Gould, R. J. 1973, Ap Letters, 14, 203
De Jager, O. C., Stecker, F. W., and Salamon, M. H. 1994, Nature, 369, 294
Dermer, C. D., and Schlickeiser, R., 1993, ApJ, 416, 458
Dermer, C. D., and Schlickeiser, R., 1994, ApJS, 90, 945
Dermer, C. D., and Gehrels, N., 1995, ApJ, in press
Fichtel, C. E., et al. 1994, ApJS, 94, 551
Gould, R. J., and Schréder, G. P. 1967, Phys. Rev., 155, 1404
Kerrick, A. D., et al. 1995, ApJ Letters, 438, L59
Kikuchi, S., and Mikami, Y. 1987, PASJ, 39, 237
MacMinn, D., & Primack, J. 1994, preprint
Macomb, D. J. et al. 1995, in preparation
Peterson, B. M., et al. 1991, ApJ, 369, 119
Punch, M., et al., 1992, Nature, 358, 477 (1992)
Salamon, M. H., Stecker, F. W., & De Jager, O. C. 1994, ApJ, 423, L1
Schubnell, M., et al. 1993, in The Second Compton Symposium, ed. C. E. Fichtel, N. Gehrels, and J. P. Norris, (New York: AIP), p. 597
Sikora, M., Begelman, M. C., and Rees, M. J. 1994, ApJ, 421, 153
Stecker, F. W., and de Jager, O. C. 1993, ApJ, 415, L71
Stecker, F. W., de Jager, O. C., and Salamon, M. H. 1992, ApJ, 390, L49
Takahashi, T., et al. 1994, IAU Circular No. 5993, 1994 May 23
White, T. R., & Lightman, A. P. 1990, ApJ, 352, 495

This article was processed by the author using Springer-Verlag
LaTeX A&A style file *L-AA* version 3.

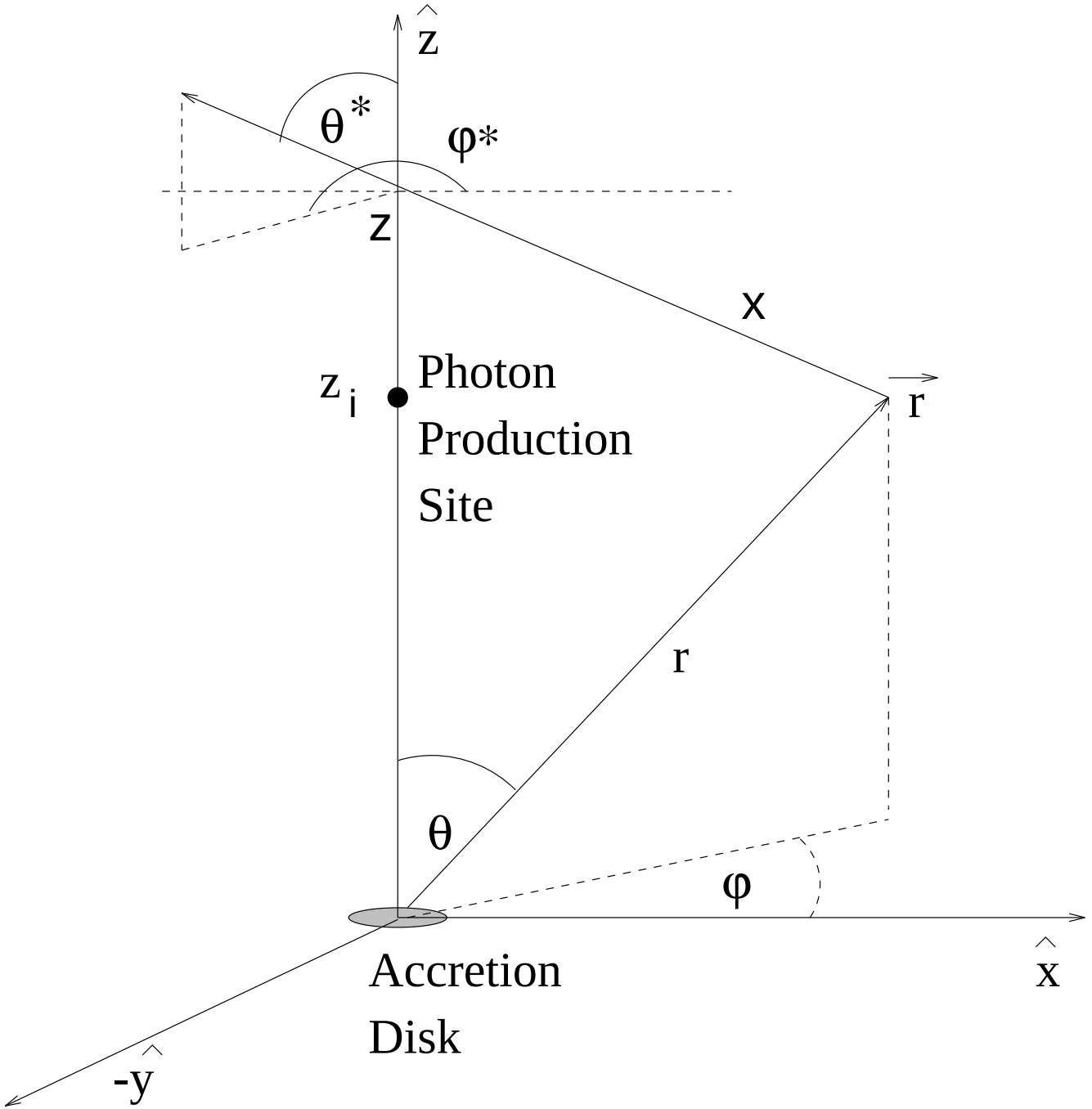
ẑ
θ*
φ*
z
x
z_i
Photon
Production
Site
r
r
θ
φ
Accretion
Disk
x̂
-ŷ

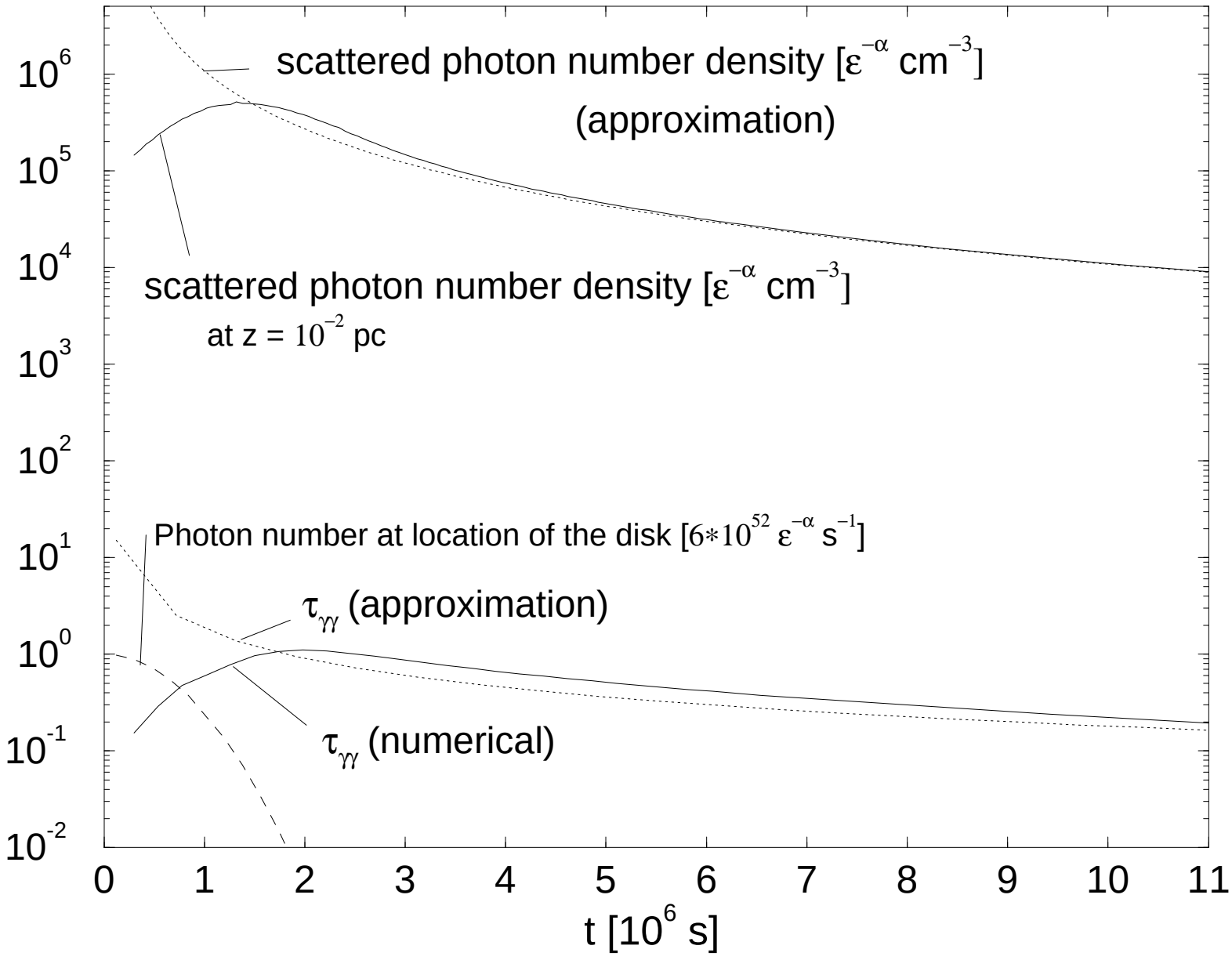
scattered photon number density [ε^−α cm^−3]
(approximation)
scattered photon number density [ε^−α cm^−3]
at z = 10^−2 pc
Photon number at location of the disk [6∗10^52 ε^−α s^−1]
τγγ (approximation)
τγγ (numerical)
10^6
10^5
10^4
10^3
10^2
10^1
10^0
10^-1
10^-2
0
1
2
3
4
5
6
7
8
9
10
11
t [10^6 s]

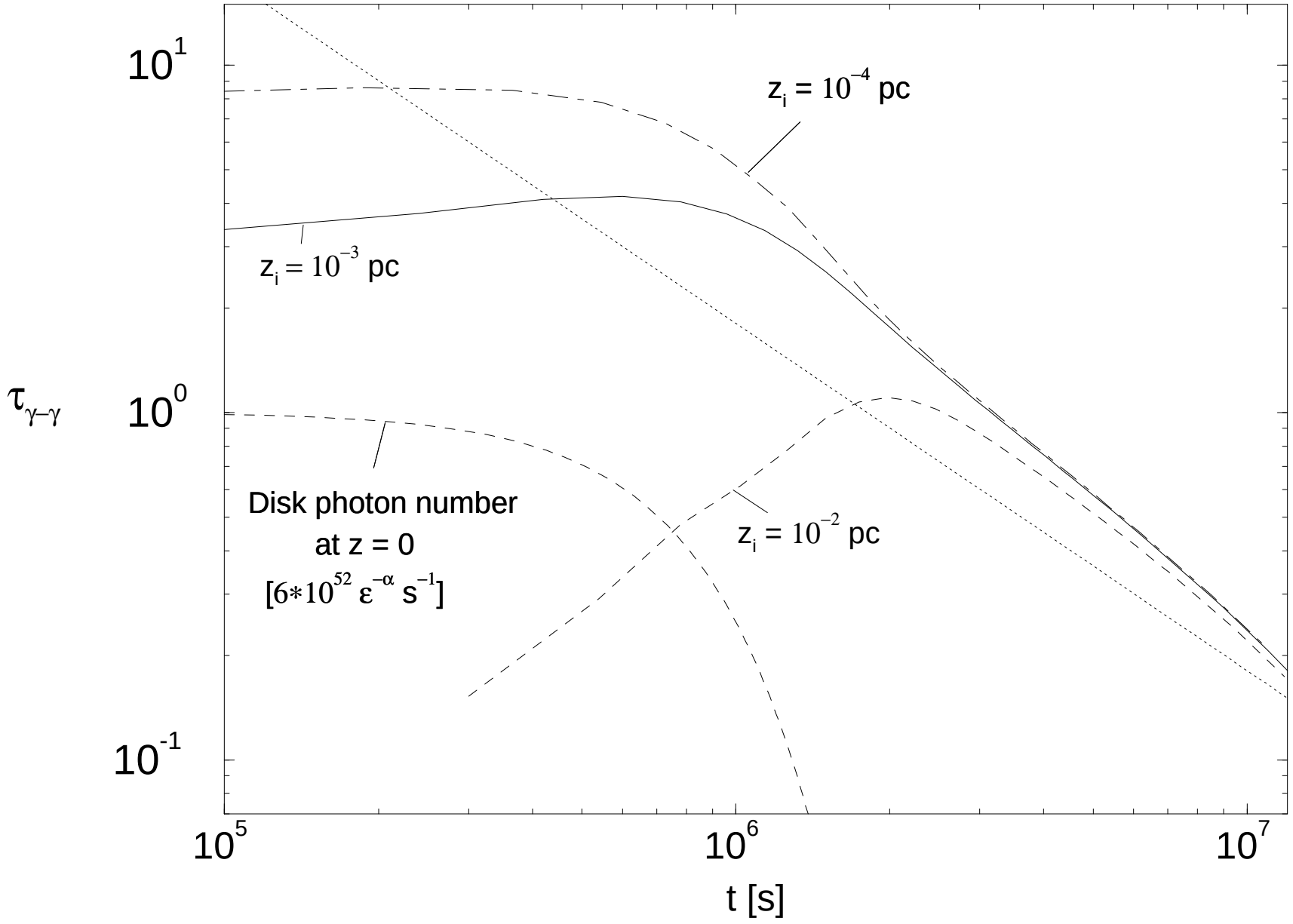
10^1
10^0
10^{-1}
$\tau_{\gamma-\gamma}$
$z_i = 10^{-4}$ pc
$z_i = 10^{-3}$ pc
$z_i = 10^{-2}$ pc
Disk photon number
at z = 0
$[6*10^{52}\ \varepsilon^{-\alpha}\ s^{-1}]$
10^5
10^6
10^7
t [s]

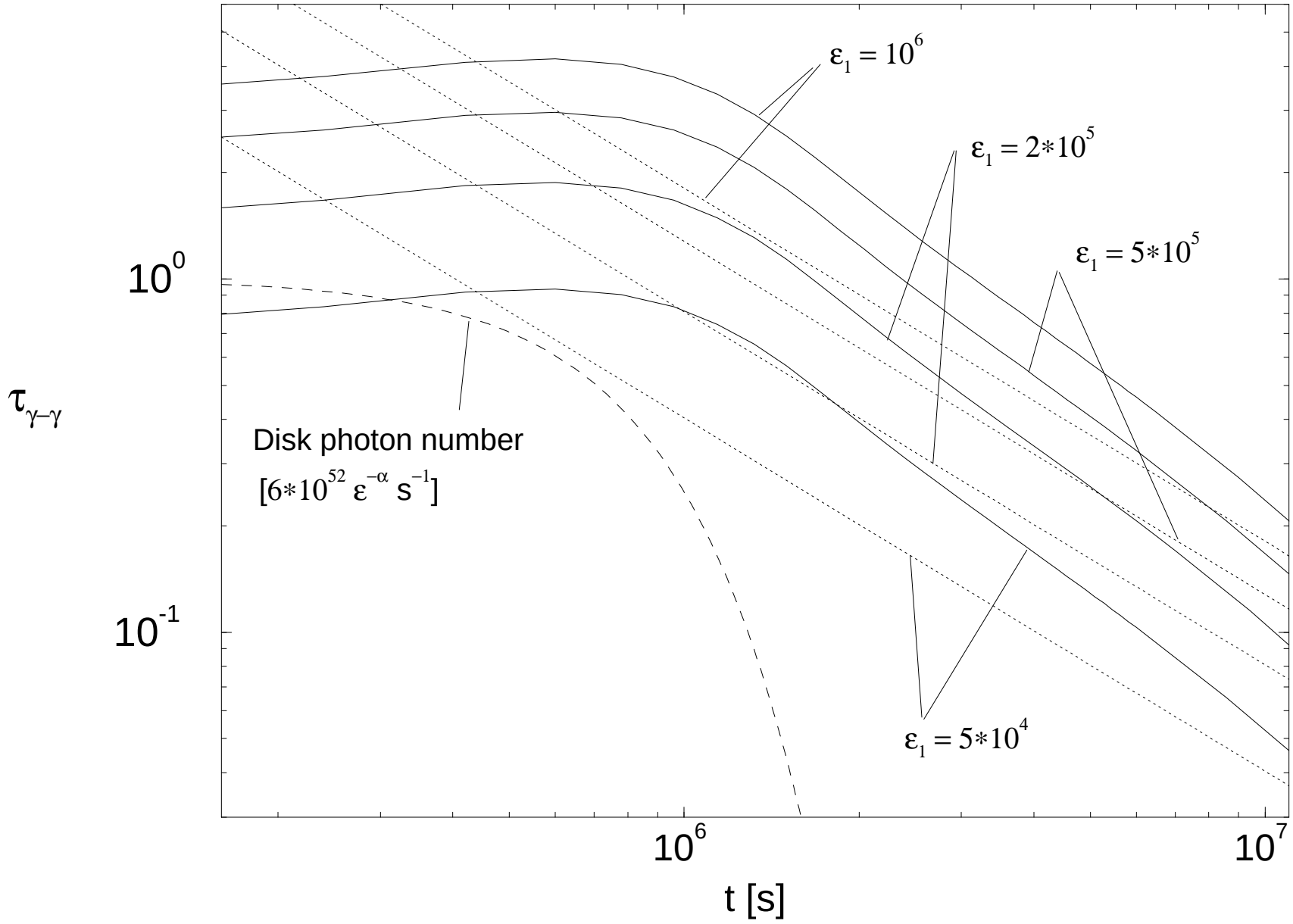
$\varepsilon_1 = 10^6$
$\varepsilon_1 = 2*10^5$
$\varepsilon_1 = 5*10^5$
$\varepsilon_1 = 5*10^4$
Disk photon number
$[6*10^{52}\ \varepsilon^{-\alpha}\ s^{-1}]$
10^0
10^{-1}
$\tau_{\gamma-\gamma}$
10^6
10^7
t [s]

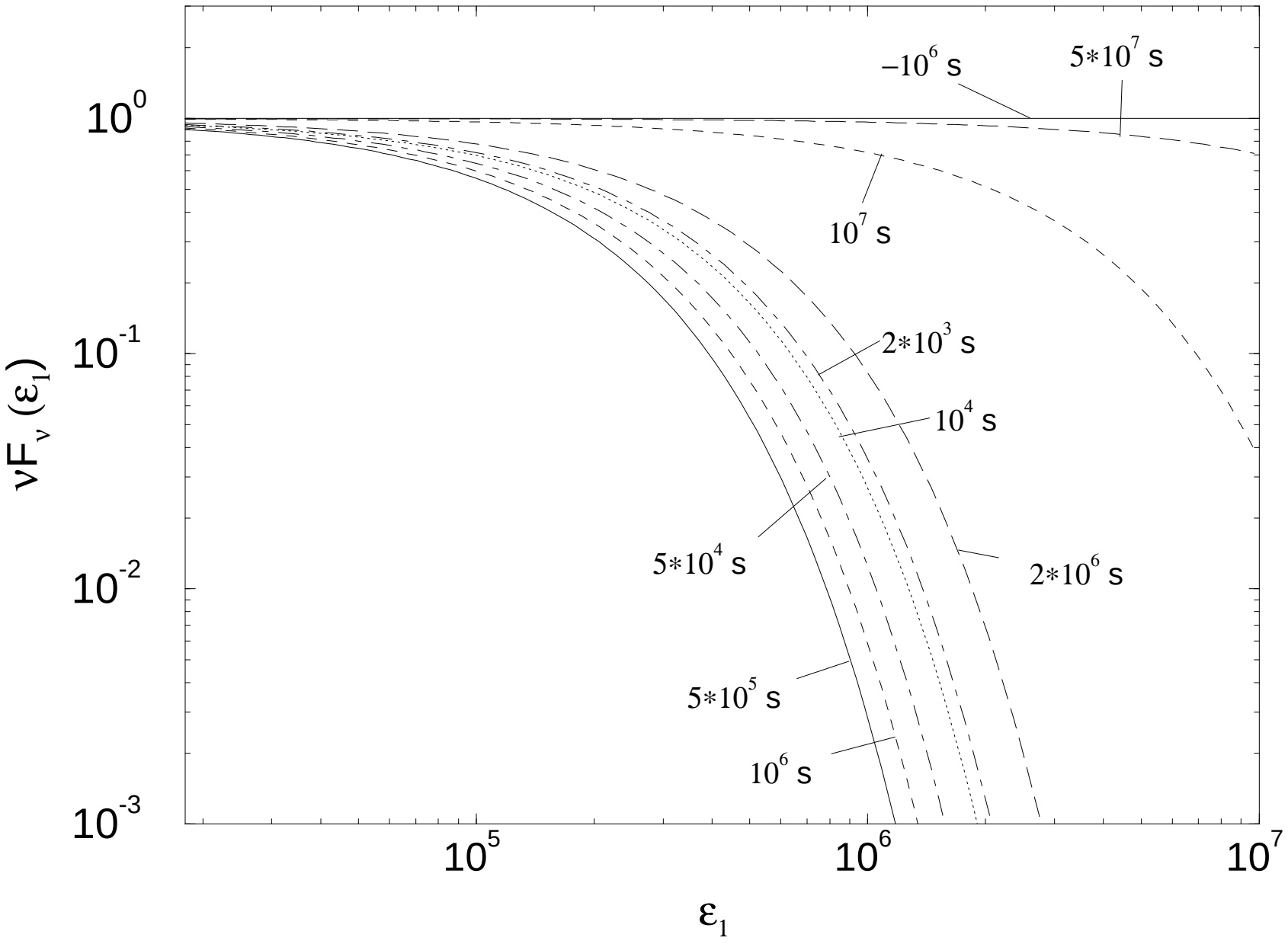
10^0
10^{-1}
10^{-2}
10^{-3}
$\nu F_\nu\ (\varepsilon_1)$
10^5
10^6
10^7
ε_1
-10^6 s
$5*10^7$ s
10^7 s
$2*10^3$ s
10^4 s
$5*10^4$ s
$2*10^6$ s
$5*10^5$ s
10^6 s